The origins of stability of spontaneous vesicles

H. T. Jung*, B. Coldren*, J. A. Zasadzinski*†, D. J. Iampietro‡, and E. W. Kaler‡

*Department of Chemical Engineering and Materials Research Laboratory, University of California, Santa Barbara, CA 93106-5080; and ‡Center for Molecular and Engineering Thermodynamics, Department of Chemical Engineering, University of Delaware, Newark, DE 19716

Equilibrium unilamellar vesicles are stabilized by one of two distinct mechanisms depending on the value of the bending constant. Helfrich undulations ensure that the interbilayer potential is always repulsive when the bending constant, K, is of order k_BT. When $K \gg k_BT$, unilamellar vesicles are stabilized by the spontaneous curvature that picks out a particular vesicle radius; other radii are disfavored energetically. We present measurements of the bilayer elastic constant and the spontaneous curvature, R_o, for three different systems of equilibrium vesicles by an analysis of the vesicle size distribution determined by cryo-transmission electron microscopy and small-angle neutron scattering. For cetyltrimethylammonium bromide (CTAB)/sodium octyl sulfonate catanionic vesicles, $K = .7\ k_BT$, suggesting that the unilamellar vesicles are stabilized by Helfrich-undulation repulsions. However, for CTAB and sodium perfluorooctanoate (FC$_7$) vesicles, $K = 6\ k_BT$, suggesting stabilization by the energetic costs of deviations from the spontaneous curvature. Adding electrolyte to the sodium perfluorooctanoate/CTAB vesicles leads to vesicles with two bilayers; the attractive interactions between the bilayers can overcome the cost of small deviations from the spontaneous curvature to form two-layer vesicles, but larger deviations to form three and more layer vesicles are prohibited. Vesicles with a discrete numbers of bilayers at equilibrium are possible only for bilayers with a large bending modulus coupled with a spontaneous curvature.

Understanding the magnitude and origin of the forces between bilayer membranes is essential to understanding the stability of unilamellar vesicles against adhesion and fusion (1). This is important especially for differentiating between metastable mechanically or chemically formed unilamellar vesicles [the equilibrium form of which is often a multilayered lamellar phase (2) or multilayered liposomes (3, 4)] and equilibrium unilamellar vesicles (5–17). Unilamellar vesicles can be stabilized against formation of multilamellar liposomes by either (*i*) thermal fluctuations that lead to a net repulsive interaction between bilayers (18) or (*ii*) a spontaneous curvature that picks out a particular vesicle radius with other bilayer curvatures being prohibited energetically (7–9). In mechanism *i*, bilayer fluctuations induce a repulsive potential between bilayers of spacing δ (18),

$$E_{\text{fluct}} = \frac{3\pi^2}{128} \frac{(k_BT)^2}{\kappa\delta^2},\qquad [1]$$

that can overwhelm the van der Waals attraction between bilayers [which is also proportional to δ^{-2} when κ is small, leading to stable unilamellar vesicles, especially when combined with electrostatic repulsion in charged systems (10)]. Theory and experiments have shown that surfactant mixing can lead to sufficiently low values of κ (10, 19, 20).

For mechanism *ii*, nonideal surfactant mixing can cause the interior and exterior monolayers of the vesicle bilayer to have different compositions, leading to a spontaneous bilayer curvature (8, 9). If the bilayers are sufficiently rigid (κ ≫ k_BT), the curvature energy of adding a second bilayer to the vesicle can overcome the attractive interaction between bilayers, leading to unilamellar vesicles. However, although the concept of spontaneous curvature is well accepted theoretically (8, 9, 21), there has been no definitive experimental proof of a spontaneous curvature in bilayers at equilibrium (22).

To distinguish between these two mechanisms of vesicle stability, we have measured the bending elasticity and bilayer spontaneous curvature in three different systems of spontaneous unilamellar vesicles (7) by analysis of the vesicle size distribution (23). Vesicles formed spontaneously after gentle mixing of micellar solutions of cetyltrimethylammonium bromide (CTAB; Aldrich) with sodium octyl sulfonate (SOS; Aldrich), CTAB with sodium perfluorooctanoate (FC$_7$; PCR Research Chemicals, Gainesville, FL) or CTAB with sodium perfluorohexanoate (FC$_5$, perfluorohexanoic acid; TCI America, Portland, OR) was neutralized with NaOH to give the sodium salt. Samples were prepared by first mixing stock solutions of each surfactant with water (or water with 1 wt % NaBr) to the desired surfactant wt %. The stock solutions were combined in the appropriate weight fractions and allowed several weeks to equilibrate. Although it is difficult to prove that vesicles formed from these mixtures at equilibrium, the composition and extent of the vesicle phase was reproducible regardless of the sample history or mixing path, and the vesicle size distributions were stable for months (7, 24).

The equilibrium size distribution of a population of vesicles is determined by a subtle competition between the entropy of mixing and the curvature elasticity of the bilayers (1, 10, 25, 26). The curvature energy per unit area of bilayer, f_c, is (8, 9, 21):

$$f_c = \frac{1}{2}\kappa\left(\frac{1}{R_1} + \frac{1}{R_2} - \frac{2}{R_o}\right)^2 + \bar{\kappa}\left(\frac{1}{R_1R_2}\right)\qquad [2]$$

where R_1 and R_2 are the principle radii of curvature, κ is the curvature modulus, and $\bar{\kappa}$ is the saddle-splay modulus. The spontaneous curvature, $1/R_o$, is nonzero only if there is asymmetry between the different sides of the bilayer (8, 9, 21). There are a limited number of measurements of κ for vesicle-forming membranes; double-tailed phospholipid bilayers range from $10k_BT < \kappa < 40k_BT$ (27–32). For highly swollen surfactant lamellar (10, 33–35) and microemulsion (36, 37) phases, $\kappa \approx k_BT$. There are even fewer measurements of the saddle-splay modulus (10) and the spontaneous curvature (22).

For the spherical vesicles studied here, $R_1 = R_2 = R$, and Eq. **2** can be simplified (8, 9, §):

$$f = 2K\left(\frac{1}{R} - \frac{1}{R_o}\right)^2$$

$$2K = 2\kappa + \bar{\kappa}$$

$$R_o = \frac{2\kappa + \bar{\kappa}}{2\kappa}R_o\qquad [3]$$

ENGINEERING

R_o is the radius of the minimum-energy vesicle, and K is an effective bending constant (8, 9). As $\bar{\kappa} < 0$ for structures that prefer a spherical shape, K is a lower bound for κ for vesicles (10, 38). The distribution of surfactant between vesicles of aggregation number M, corresponding to the minimum energy radius, R_o ($M = 8\pi R_o^2/A_o$, in which A_o is the mean molecular area), relative to vesicles of aggregation number N and radius R, is dictated by a balance between the entropy of vesicle mixing and the curvature energy (1):

$$\frac{X_N}{N} = \left\{ \frac{X_M}{M}\exp\left[\frac{M(\mu_M^0 - \mu_N^0)}{k_B T}\right] \right\}^{\frac{N}{M}} \quad [4]$$

X_M, μ_M^0, and X_N, μ_N^0 are the mole fraction of surfactant and the standard chemical potential per molecule in vesicles of size M and N, respectively. Eq. 4 assumes ideal mixing of the vesicles (not the molecules within the bilayers) and is valid for dilute vesicle dispersions in which the Debye length is small in comparison to the intervesicle distance (39, ¶). The chemical potential difference is due to the change in curvature energy per molecule for surfactant distributed between vesicles of different radii:

$$(\mu_N^0 - \mu_M^0) = \frac{4\pi R^2 f}{N} = \frac{8\pi K\left(1 - \dfrac{R}{R_o}\right)^2}{N} \quad [5]$$

Inserting Eq. 5 into Eq. 4 and substituting $M = 8\pi R_o^2/A_o$ and $N = 8\pi R^2/A_o$ gives the vesicle size distribution as a function of R_o and K (1, 30):

$$C_N = \left\{ C_M \exp\left[\frac{-8\pi K}{k_B T}\left(1 - \frac{R_o}{R}\right)^2\right] \right\}^{\frac{R^2}{R_o^2}} \quad [6]$$

where C_M ($= X_M/M$) and C_N are the molar or number fractions of vesicles of size M and N, respectively. A consequence of Eq. 6 is that vesicles stabilized by thermal fluctuations ($K \approx k_B T$) have a much broader size distribution than vesicles stabilized by the spontaneous curvature ($K \gg k_B T$). This result is the opposite of vesicle size distribution models that do not include a spontaneous curvature (10, 40).

To extract R_o and K, it is necessary to determine the vesicle size distribution by cryo-transmission electron microscopy (TEM). For cryo-TEM, a thin (<1-μm) layer of the vesicle liquid is spread on a lacey carbon grid (Ted Pella, Redding, California) in a temperature-controlled chamber saturated with the vesicle solution of interest. The grid is plunged into a mixture of liquid ethane and liquid propane cooled by liquid nitrogen (23). The frozen samples are transferred to a GATAN (Pleasanton, CA) cold stage and imaged directly at 100 kV by using a JEOL 100CXII. Bright-field phase-contrast TEM micrographs were recorded by using standard low-dose procedures on either film or a GATAN CCD camera.

Fig. 1A is a cryo-TEM image of a vesicle dispersion containing 2 total wt % of 3:7 CTAB/SOS in water. In cryo-TEM images, unilamellar vesicles appear as uniformly dark circular rings; contrast in the image is generated by the variation of the projection of the electron beam, which is normal to the image in these figures, through the vesicle membrane. Where the vesicle
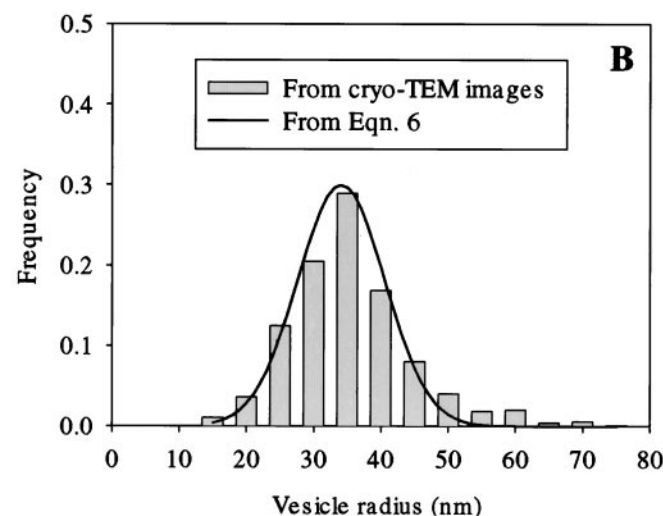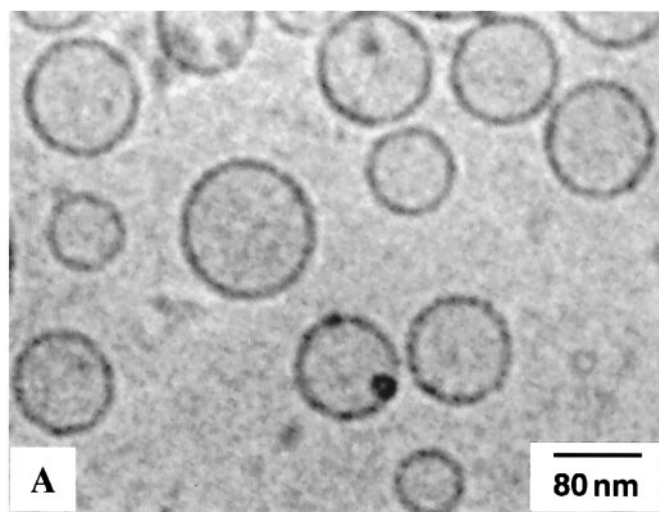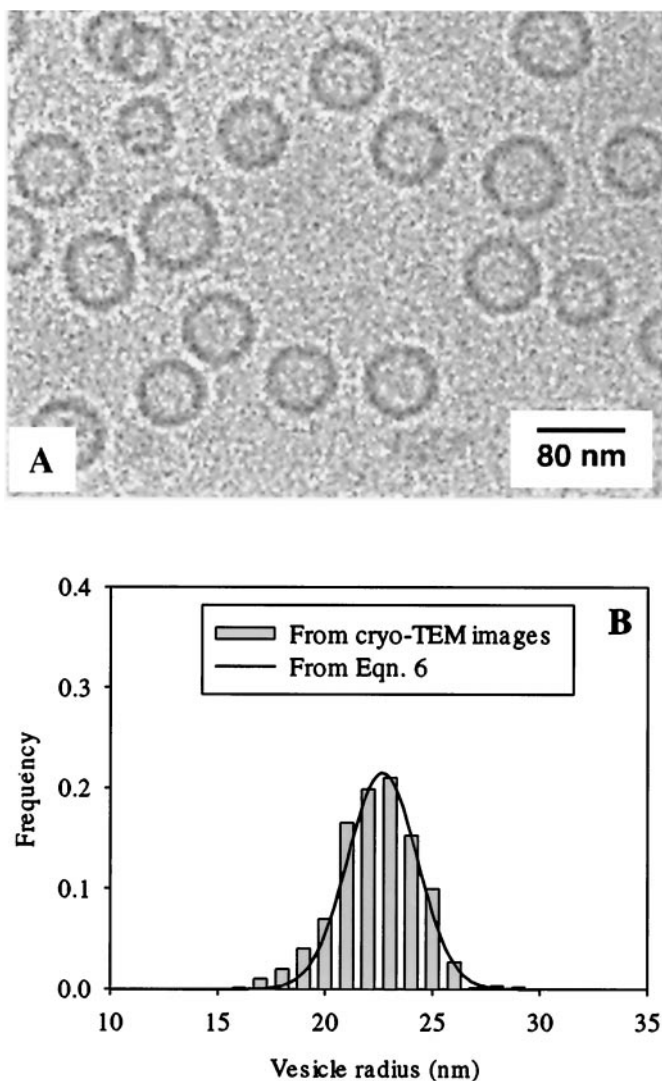

Fig. 1. (*A*) Cryo-TEM image of CTAB/SOS/water (2 wt % total surfactant, CTAB/SOS ratio of 3:7 by weight) system showing unilamellar vesicles with a broad size distribution. The vesicles are polydisperse, with the average radius of 37 nm and a standard deviation of 10 nm. (*B*) Vesicle size distribution histogram determined from measurements of about 3,000 vesicles from many different samples and cryo-TEM images. There are a few much larger vesicles (100–500 nm) in this mixture, but the fraction is so small that they were not plotted in the histogram. The solid line is a fit to Eq. 6 with $R_o = 37$ nm and $K = 0.7 \pm 0.2$ $k_B T$.

bilayer is oriented parallel to the electron beam (edges of the vesicle), the projection through the bilayer is greater than where the bilayer is perpendicular to the electron beam (center of the vesicle). The width of the dark rim of the vesicle is wider than the actual bilayer thickness because of the curvature of the vesicle. A histogram of the size distribution was built up by measuring the size of ≈3,000 spherical vesicles taken from many different samples over several weeks (Fig. 1B). The measured distribution was fit to Eq. 6 (solid line) to determine R_o and K and showed excellent agreement with the equilibrium distribution. The best fit to Eq. 6 gives $K = 0.7 \pm 0.2$ $k_B T$ and $R_o = 37$ nm.
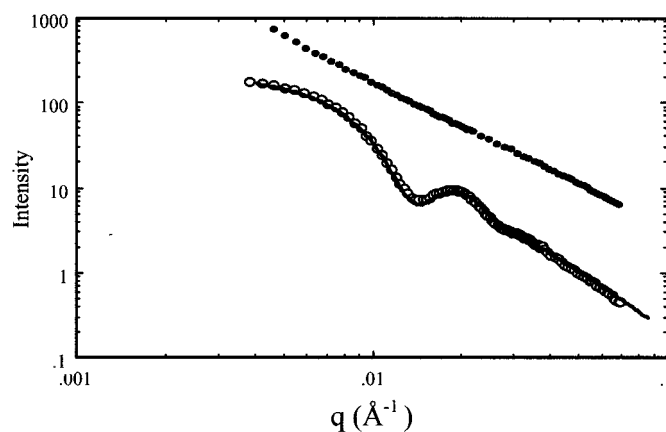
Fig. 2A shows that the vesicles in a 2 wt % 2:8 CTAB/FC$_7$ dispersion are smaller, and the size distribution (Fig. 2B) is much narrower than that of the CTAB/SOS dispersion (Fig. 1B). In addition to the spherical vesicles, there were also a small number

---

¶The minimum ionic strength of these catanionic solutions is equal to the concentration of the minor surfactant component, and the maximum is the total surfactant concentration (see refs. 7 and 24). For these experiments, the ionic strength ranges from ≈10–100 mM. This ionic strength leads to a Debye length of 1–10 nm (see chapter 12 of ref. 42), a small fraction of the average intervesicle spacing (as seen in the micrographs) of 75–100 nm. Hence, electrostatic interactions are negligible between the vesicles, and the ideal mixing approximation in Eq. 4 is justified.

Fig. 3. SANS spectra (open circles) for CTAB/FC$_7$ vesicles (2 wt % total surfactant, CTAB/FC$_7$ ratio of 2:8 by weight; see Fig. 2). The expected q^{-2} dependence for hollow spheres is observed for q > 0.04 Å^{-1}. A distinct minimum is present over the range 0.01 < q < 0.02 Å^{-1}. The solid lines through the data represent the best fit of a simple hollow-sphere model with three adjustable parameters: the average inner-vesicle radius, the bilayer thickness, and the polydispersity. The model results yield outer-vesicle radii between 23 and 24 nm, a bilayer thickness of 2.8 nm, and a polydispersity of 17%. These results are in remarkable agreement with the size distribution measured by TEM (Fig. 2), which also shows a monodisperse population with an average radius of 23 nm. This data is to be compared with the neutron scattering from CTAB/SOS vesicles (solid circles, ×10) that only show the expected q^{-2} dependence with no characteristic minimum (Fig. 1). This result indicates a more polydisperse sample also in good agreement with the TEM data. Neutron-scattering experiments were performed by using the NG-7 spectrometer at the National Institute of Standards and Technology (NIST) in Gaithersburg, MD. Neutrons with wavelength of 6 Å (with a spread of $\Delta\lambda/\lambda = 0.10$) and 3 sample-to-detector distance (1.0, 4.5, and 13.0 m) were used with the detector on axis for the long distance and offset 25 cm for the two shorter distances. These configurations produced a scattering vector range of 0.005 to 0.50 Å^{-1}. Samples were transferred into quartz scattering cells (0.2-cm path length) and equilibrated in a temperature-controlled heating block before measurement. The scattered intensity was corrected for background scattering as well as detector efficiency and placed on absolute scale by using standards provided by the NIST.

Fig. 2. (A) Cryo-TEM image of CTAB/FC$_7$ (2 wt % total surfactant, CTAB/FC$_7$ ratio of 2:8 by weight) vesicle system with a significantly more narrow size distribution than the CTAB/SOS vesicles in Fig. 1. All of the vesicles were unilamellar under these conditions. The vesicle phase exists on the FC$_7$- (and FC$_5$-) rich side at concentrations between ≈2 and 4 wt % surfactant and for mixing ratios greater than 80% FC$_7$ (and FC$_5$). (B) Vesicle size distribution histogram determined from the cryo-TEM images; the solid line is a fit to Eq. 6 with $R_o = 23$ nm and $K = 6 \pm 2 \, k_B T$.

of cylindrical vesicles (with radius equal to the spherical-vesicle radius) and some open discs (not shown). Fitting the distribution of spherical vesicles to Eq. 6 also results in remarkably good agreement between the experimental and theoretical distributions, with $R_o = 23$ nm and $K = 6 \pm 2 \, k_B T$, indicating that the hydrocarbon–fluorocarbon (CTAB/FC$_7$) bilayers are much stiffer than the hydrocarbon–hydrocarbon bilayers (CTAB/SOS). Other systems of perfluorinated surfactants with hydrocarbon surfactants also show monodisperse vesicles (14). Replacing the FC$_7$ fluorocarbon surfactant with the shorter-chain FC$_5$ lowers the bending modulus of the resulting vesicles to $K = 0.5 \, k_B T$ but increases R_o to 56 nm. The morphology of the sample is similar to the CTAB/SOS system, showing a broad vesicle size distribution (data not shown). Single-parameter models of the vesicle size distribution that depend on the bending energy but do not include a spontaneous curvature term (10, 40) cannot fit the experimental distribution for either the CTAB/SOS or CTAB/FC$_7$ vesicles.

To verify the accuracy of the TEM size distribution, small-angle neutron scattering (SANS) was performed (Fig. 3). The SANS data for the CTAB/FC$_7$ vesicles showed a minimum in the range 0.01 < q < 0.02 A, which is characteristic of the form factor for a monodisperse population of spherical vesicles with mean radii of 23–24 nm. This result is in excellent quantitative agreement with the TEM size distribution. There has been some speculation in the literature that the vesicle size distribution is the result of shear forces during preparation (2). This speculation clearly is not the case for the vesicle systems examined here, because the samples for TEM undergo significant shear to make the thin (100-nm) films necessary for imaging, whereas the SANS samples are unsheared (23); however, the size distributions are identical. The SANS spectra for CTAB/SOS is featureless, indicative of a polydisperse population of vesicles also in agreement with the TEM data.

Given the large difference in the bilayer properties, it is likely that the stabilization mechanism is different as well. For the CTAB/SOS and CTAB/FC$_5$ systems, thermal undulations (Eq. 1) caused by the small value of K stabilize the hydrogenated vesicles against formation of multilamellar liposomes, even in the absence of electrostatics. Previous work has shown that CTAB/SOS vesicles are stable even with 1.4 wt % added salt, at which point a phase transition to micelles occurs (24). The large bending constant and narrow size distribution suggest that CTAB/FC$_7$ vesicles are stabilized by the energy costs of deviations from the spontaneous curvature.

ENGINEERING
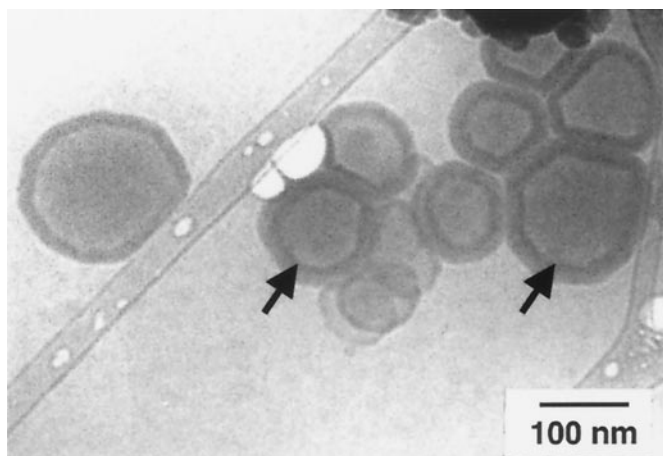
Fig. 4. Cryo-TEM image of CTAB/FC$_7$ (2 wt % total surfactant, CTAB/FC$_7$ ratio of 2:8 by weight) in 1 wt % NaBr. Two-layer vesicles are distinguished from one-layer vesicles (Figs. 1 and 2) by the darker rim on the inside edge of the vesicle membrane (arrows). This dark inside rim is caused by the increased projection of the electron beam through both the interior and exterior vesicle bilayers; the single-bilayer vesicles in Figs. 1 and 2 have membranes with a uniform intensity and do not show the interior dark rim. From examining many images, about 90% of the vesicles with added salt have two bilayers, and the rest appear to have one bilayer. There were essentially no vesicles with three layers or more. The vesicles in the 1% NaBr sample also had a greater tendency to adhere both to each other and the polymer-coated electron microscope grid (23) and flatten, consistent with the enhanced attraction between the vesicle bilayers (41). Some of the vesicles are clustered and appear polygonal; the vesicles can come into closer proximity because of the screening of the residual electrostatic forces, indicative of the net attractive forces between the bilayers. Although the vesicles cluster, they maintain a discrete number of bilayers.

A consequence of stabilization by spontaneous curvature is the possibility of vesicles with a discrete number of bilayers depending on the magnitude and sign of the bilayer interactions. When 1 wt % NaBr was added to screen any residual short-range electrostatic interactions between the bilayers, the result was the spontaneous formation of a population of primarily two-layered vesicles (Fig. 4). In Fig. 4, two-layer vesicles are distinguished from one-layer vesicles (Figs. 1 and 2) by the darker rim on the inside edge of the apparent vesicle membrane (arrows). This dark rim is caused by the greater projection of the electron beam through both the interior and exterior vesicle bilayers; the single-bilayer vesicles in Figs. 1 and 2 have membranes with a uniform intensity and do not show the interior dark rim. From examining many images, about 90% of the vesicles with added salt have two bilayers, whereas the rest have one bilayer. There were essentially no vesicles with three layers or more. The vesicles in 1% NaBr sample also had a greater tendency to adhere both to each other and the carbon-coated electron microscope grid (23) and flatten, consistent with the enhanced attraction between the vesicle bilayers (41).

The distribution between one-layer and two-layer vesicles can be derived by using the mass action model, Eq. **4**, for vesicles with a spontaneous bilayer curvature. A two-layer vesicle, with the outer bilayer of radius R_1 and inner bilayer of radius R_o (the spontaneous radius of curvature), can be compared with two vesicles, both of radius R_o. The aggregation number N of the two-layer vesicle is approximately twice that of a one-layer vesicle, M: $N \approx 2M$. The outer-vesicle radius, R_1, can be expressed in terms of the bilayer thickness, t, the bilayer separation, δ, and R_o, $R_1 = R_o + (t + \delta)$; the curvature energy of the vesicles of radius R_o is zero, whereas the curvature energy per molecule of the vesicle with the outer bilayer of radius R_1 is (from Eqs. **3** and **5**):

$$E_{\text{curvature}} = \frac{8\pi K}{N}\left(\frac{t + \delta}{R_o}\right)^2 \qquad [7]$$

Typical contributions to the interaction energy, $\Gamma(\delta)$, only depend on the separation between bilayers (40). The distribution between one-bilayer and two-bilayer vesicles is:

$$C_2 = C_1^2 \exp\left[\frac{-1}{k_B T}\left(8\pi K\left(\frac{t + \delta}{R_o}\right)^2 + \Gamma(\delta)\right)\right] \qquad [8]$$

C_1 ($= X_1/M$) and C_2 are the mole fractions of unilamellar and two-layer vesicles, respectively. For the surfactant concentrations used in these experiments, the vesicle mole fraction $C_1 \approx 10^{-6}$, so in the absence of attractive interactions, there are only unilamellar vesicles.

At high-salt concentration, $\Gamma(\delta)$ can be approximated by the sum of the van der Waals attraction and the Helfrich undulation interaction (Eq. **1**):

$$\Gamma_1(\delta) \approx (4\pi R_o^2)\left[\frac{-A_0}{12\pi\delta^2} + \frac{3\pi^2}{128}\frac{(k_B T)^2}{\kappa\delta^2}\right] \approx -A_{\text{eff}}\frac{R_o^2}{\delta^2} \qquad [9]$$

in which A_{eff} can be considered an effective Hamaker constant, which we estimate as 0.17 $k_B T$ (42). For reasonable values of $t \approx$ 3 nm, d $\approx$ 2 nm, $R_o = 23$ nm, and $K = 6\,k_B T$, $8\pi K[(t + \delta)/R_o]^2 - A_{\text{eff}}(R_o^2/\delta^2 \approx -16 k_B T$, and from Eq. **9**, $C_2 \approx 10 C_1$. Similar approximations for three-layer vesicles with the same parameters give $C_3 \approx 0.01C_1 \approx 0.001C_2$. Hence, there should be many more two-layer vesicles than one-layer vesicles and essentially no three-layer vesicles, consistent with Fig. 4. Extending the calculation to four- or more-layer vesicles shows there is a negligible fraction at this overall surfactant concentration.

Although the parameter values are estimates, the analysis shows that vesicles stabilized by spontaneous curvature can have a narrow distribution of the number of bilayers when the attractive interactions just balance the curvature energy. In the absence of a spontaneous bilayer curvature, each additional layer added to a vesicle has a decreasing curvature energy, but the attractive interaction energy grows with the net bilayer area in contact, and a polydisperse population of multilamellar liposomes results. Hence, typical phospholipid vesicles, with $1/R_o = 0$, are unstable relative to multilamellar liposomes. The combination of a narrow size distribution, a large bending elastic constant, and the formation of two-bilayer vesicles shows that the CTAB/FC$_7$ vesicles are stabilized by spontaneous curvature.

1. Israelachvili, J. N., Mitchell, D. J. & Ninham, B. W. (1976) *J. Chem. Soc. Faraday Trans. 2* **72,** 1526–1568.
2. Horbaschek, K., Hoffmann, H. & Hao, J. (2000) *J. Phys. Chem. B* **104,** 2781–2784.
3. Szoka, F. & Papahadjopoulos, D. (1980) *Annu. Rev. Biophys. Bioeng.* **9,** 467–508.
4. Lasic, D. D. (1993) *Liposomes: From Physics to Applications* (Elsevier Science, Amsterdam).
5. Hargreaves, W. R. & Deamer, D. W. (1978) *Biochemistry* **17,** 3759–3768.
6. Talmon, Y., Evans, D. F. & Ninham, B. W. (1983) *Science* **221,** 1047–1049.
7. Kaler, E. W., Murthy, A. K., Rodriguez, B. E. & Zasadzinski, J. A. N. (1989) *Science* **245,** 1371–1374.
8. Safran, S. A., Pincus, P. & Andelman, D. (1990) *Science* **248,** 354–355.
9. Safran, S. A., Pincus, P. A., Andelman, D. & MacKintosh, F. C. (1991) *Phys. Rev. A At. Mol. Opt. Phys.* **43,** 1071–1078.
10. Herve, P., Roux, D., Bellocq, A. M., Nallet, F. & Gulik-Krzywicki, T. (1993) *J. Phys. II* **3,** 1255–1270.

11. Hoffmann, H., Thunig, C., Munkert, U., Meyer, H. W. & Richter, W. (1992) *Langmuir* **8,** 2629–2638.
12. Ambuhl, M., Bangerter, F., Luisi, P. L., Skrabal, P. & Watzke, H. J. (1993) *Langmuir* **9,** 36–38.
13. Chiruvolu, S., Warriner, H. E., Naranjo, E., Idziak, S., Radler, J. O., Plano, R. J., Zasadzinski, J. A. & Safinya, C. R. (1994) *Science* **266,** 1222–1225.
14. Ristori, S., Appell, J. & Porte, G. (1996) *Langmuir* **12,** 686–690.
15. Murthy, K., Easwar, N. & Singer, E. (1998) *Colloid Polym. Sci.* **276,** 940–944.
16. Martinez, J. S., Zhang, G. P., Holt, P. D., Jung, H.-T., Carrano, C. J., Haygood, M. G. & Butler, A. (2000) *Science* **287,** 1245–1247.
17. Viseu, M. I., Edwards, K., Campos, C. S. & Costa, S. M. B. (2000) *Langmuir* **16,** 2105–2114.
18. Helfrich, W. (1978) *Z. Naturforsch., A* **33,** 305–315.
19. Szleifer, I., Ben-Shaul, A. & Gelbart, W. M. (1990) *J. Phys. Chem.* **94,** 5081–5089.
20. Szleifer, I., Kramer, D., Ben-Shaul, A., Gelbart, W. M. & Safran, S. A. (1990) *J. Chem. Phys.* **92,** 5081–5089.
21. Helfrich, W. (1973) *Z. Naturforsch., C* **28,** 693–703.
22. Doebereiner, H. G., Selchow, O. & Lipowsky, R. (1999) *Eur. Biophys. J.* **28,** 174–178.
23. Chiruvolu, S., Naranjo, E. & Zasadzinski, J. A. (1994) in *ACS Symposium Series*, eds. Herb, C. A. & Prud'homme, R. K. (Am. Chem. Soc., Washington, DC), Vol. 578.
24. Brasher, L. L., Herrington, K. L. & Kaler, E. W. (1995) *Langmuir* **11,** 4267–4277.
25. Morse, D. C. & Milner, S. T. (1995) *Physical Review E Stat. Phys. Plasmas Fluids Relat. Interdisc. Top.* **52,** 5918–5985.
26. Simons, B. D. & Cates, M. E. (1992) *J. Phys. II* **2,** 1439–1451.
27. Schneider, M. B., Jenkins, J. T. & Webb, W. W. (1984) *J. Phys. (France)* **45,** 1457–1472.
28. Schnieder, M. B., Jenkins, J. T. & Webb, W. W. (1984) *Biophys. J.* **45,** 891–899.
29. Evans, E. & Rawicz, W. (1990) *Phys. Rev. Lett.* **64,** 2094–2097.
30. Denkov, N. D., Yoshimura, H., Kouyama, T., Walz, J. & Nagayama, K. (1998) *Biophys. J.* **74,** 1409–1420.
31. Discher, B. M., Won, Y. Y., Ege, D. S., Lee, J. C. M., Bates, F. S., Discher, D. E. & Hammer, D. A. (1999) *Science* **284,** 1143–1146.
32. Rawicz, W., Olbrich, K. C., McIntosh, T., Needham, D. & Evans, E. (2000) *Biophys. J.* **79,** 328–339.
33. Safinya, C. R., Roux, D., Smith, G. S., Sinha, S. K., Dimon, P., Clark, N. A. & Bellocq, A. M. (1986) *Phys. Rev. Lett.* **57,** 2718–2721.
34. Safinya, C. R., Sirota, E. B., Roux, D. & Smith, G. S. (1989) *Phys. Rev. Lett.* **62,** 1134–1137.
35. Warriner, H. E., Keller, S. L., Idziak, S. H. J., Slack, N. L., Davidson, P., Zasadzinski, J. A. & Safinya, C. R. (1998) *Biophys. J.* **75,** 272–293.
36. Hellweg, T. & Langevin, D. (1998) *Phys. Rev. E Stat. Phys. Plasmas Fluids Relat. Interdisc. Top.* **57,** 6825–6834.
37. Eastoe, J., Sharpe, D. & Heenan, R. K. (1997) *Prog. Colloid Polym. Sci.* **105,** 340–345.
38. Safran, S. A. (1999) *Adv. Phys.* **48,** 395–448.
39. Chiruvolu, S., Israelachvili, J., Naranjo, E., Xu, Z., Kaler, E. W. & Zasadzinski, J. A. (1995) *Langmuir* **11,** 4256–4266.
40. Israelachvili, J. N. (1992) *Intermolecular and Surface Forces* (Academic, London).
41. Bailey, S., Longo, M., Chiruvolu, S. & Zasadzinski, J. A. (1990) *Langmuir* **6,** 1326–1329.

ENGINEERING